Crystal Structure, Fluorescence, and Nanostructuration Studies of the First Zn^{II} Anthracene-Based Curcuminoid

Núria Aliaga-Alcalde,*,[†] Laura Rodríguez,[‡] Marilena Ferbinteanu,[§] Petra Höfer,[∥] and Thomas Weyhermüller[∥]

[†]ICREA (Institució Catalana de Recerca i Estudis Avançats) & Universitat de Barcelona, Facultat de Química, Martí i Franquès, 1-11, 08028 Barcelona, Spain

[‡]Facultat de Química, Universitat de Barcelona, Martí i Franquès, 1-11, 08028 barcelona, Spain

[§]Inorganic Chemistry Department, University of Bucharest, Dumbrava Rosie 23, Bucharest 020462, Romania

[∥]Max-Planck-Institut für Bioanorganische Chemie, P.O. Box 10 13 65, D-45413 Mülheim an der Ruhr, Germany

S *Supporting Information*

ABSTRACT: In the following article the coordination properties of a recently reported curcuminoid 9Accm (9Accm = 1,7-(di-9-anthracene)-1,6-heptadiene-3,5-dione) with Zn^{II} are reported. Preparation, crystal structure, and fluorescence spectroscopic studies of [Zn^{II}(9Accm)$_2$(py)] (**1**) are presented, as well as preliminary AFM and confocal microscopy studies on graphite surfaces. Complex **1** is the first crystallographically characterized Zn−curcuminoid in the literature; the intrinsic features of the complex are contrasted with the free ligand, 9Accm, and [Cu^{II}(9Accm)$_2$(py)] (**2**), a similar copper system, which has been recently described by us. It is shown that complex **1** exhibits a chelation enhancement of fluorescence (CHEF) and **2** a chelation enhancement of quenching (CHEQ) with respect to the fluorescence response of the free ligand, demonstrating the highly sensitive response of 9Accm versus these two metals. All studies are supported by density functional theory (DFT) calculations.
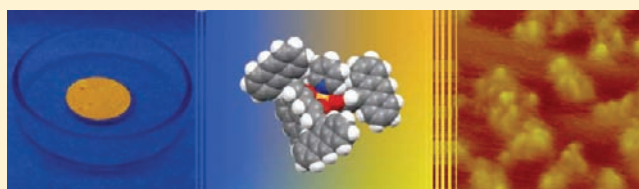
INTRODUCTION

It is well known that controlling the interaction of light and matter has a direct impact in technological advances, such as, for example, telecommunications, sensors, solar devices, medical diagnostics, and bioimaging, being nowadays one of the front-line areas of research.[1] At present, luminescent inorganic−organic hybrid materials are widely studied due to their potential application as photoluminescence and/or electroluminescence tools.[2] In this sense, anthracene-based species are promising candidates exhibiting not only luminescent (fluorescence and/or phosphorescence) but also semiconducting properties.[2a,3] The combination of such features together with their feasible deposition on substrates makes these systems of extreme interest for a range of purposes (e.g., diodes (LEDs) and photovoltaic cells).[4]

On the other hand, the photosensitive response of fluorophor groups can be affected by metal ion coordination giving rise to excellent chemosensors.[5] Upon binding, two types of optical effects have been described: chelation enhancement of quenching (CHEQ) and chelation enhancement of fluorescence (CHEF).[6] Normally, paramagnetic transition metals produce the first (where the quenching could be partial or total, e.g., Ni^{II} and Cu^{II}) and diamagnetic transition metals the second (e.g., Cd^{II} and Zn^{II}).[7] Lately, development of chemosensors for selective recognition of metal centers capable of discriminating among different analytes has attracted considerable attention, and included in this family enhancers

of the luminescence, such as, for example, Zn^{II} materials, are appealing in a number of applications.[5,8]

The present paper is an attempt to assemble anthracene chromophores with Zn^{II} ions toward development of new multifunctional systems. We design building blocks with attractive characteristics to develop hybrid functional molecules, focusing on their structural−property correlations and potential integration as (or in) molecular devices (related to nanostructuration). For that an anthracene-based curcuminoid previously designed by us was chosen; the compacted organic group contains both a binding site and fluorophor groups.[9] This organic ligand, so-called, 9Accm (1,7-(di-9-anthracene-1,6-heptadiene-3,5-dione)) possesses a diarylheptanoid backbone with a central β-diketone array and anthracene groups on the sides. 9Accm was considered in an earlier work for achievement of two new Cu^{II} compounds in which in vitro activities were studied.[9] More recently, the organic molecule by itself has been deposited on nanogap devices where its extended π-conjugated system has been proved to interact strongly with the top of graphene layers (nanoelectrodes) anchoring to them (submonolayers of 9Accm were characterized by AFM) and mediating charge transport in between.[10]

Now, our studies with Zn focus on physical characterization, fluorescent studies, and supramolecular features (on surfaces)

for development of advanced nanomaterials containing metal centers that can implement additional properties (e.g., enhancement of fluorescence) regarding their application on the above fields of molecular electronics and nanoscience. Here, the synthesis and characterization of a novel compound $[Zn(9Accm)_2(py)]$ (**1**) is described, including crystallographic, electrochemical, and fluorescent analyses. The features attained by coordination of Zn^{II} ions to the 9Accm curcuminoid are shown below as well as the studies of these species on graphite surfaces using AFM and confocal spectroscopies. These studies rise from the appealing concept that multifunctional molecules can be used at the nanoscale and the necessity of basic understanding of their deposition on different supports.

Considering the conjugate nature of 9Accm as well as incorporation of Zn^{II} ions, complex **1** could be described as a fluorophor system whose structure allows its deposition on graphite surfaces without further functionalization, anchoring on the supporting face by $\pi-\pi$ interactions. In addition, in this work we compared complex **1** with a preceding Cu^{II} analogue, $[Cu(9Accm)_2(py)]$ (for simplicity reasons described as complex **2**),[9] showing that the nature of the metal clearly modifies the characteristics of the final species (quencher). DFT calculations of both compounds have been performed with the aim of corroborating the experimental results and providing more insight on the effects on the metal−9Accm bonding. Finally, the goal of this work is to display 9Accm as an interesting ligand,[5,8d] able of providing stable species for further applications as well as unambiguous and distinctive properties depending on the metal attached to it; these initial studies are crucial toward the development of new thin-film inorganic− organic hybrid molecular materials.[1−5,11]

■ EXPERIMENTAL SECTION

Starting materials were purchased from Aldrich, and all manipulations were performed using materials as received. Ligand 9Accm and compound **2**, $[Cu(9Accm)_2(py)]$, were synthesized as reported elsewhere.[9]

Preparation of [Zn(9Accm)₂(py)] (1). The ligand, 9Accm (40 mg, 0.084 mmol), was dissolved in DMF (30 mL) and deprotonated with a solution of 0.5 M KOH (200 μL). The resulting orange solution was kept under stirring, and then, a solution of $[Zn(O_2CMe)_2(H_2O)]$ (4.5 mg, 0.025 mmol) in DMF (5 mL) was added dropwise. After 3 h of stirring a yellow-orange solid precipitated, concentrating the sample by rotary evaporation. The dry solid was washed with water, methanol, and ether and dried in the air. Finally, a yellow powder was obtained. Yield: 55%. Crystals were obtained by layering a pyridine solution of the solid with diethyl ether. IR (ν/cm^{-1}) 1629m, 1546m, 1508s, 1432s, 1410s, 1159m, 978m, 880w, 848w, 733s, 538w, 443w. ^{1}H NMR (400 MHz, CDCl₃): 8.86 (d, 4H), 8.45 (s, 4H), 8.42 (d, 8H), 8.03 (d, 8H), 7.52 (tt, 16H), 6.78 (d, 4H), 5.94 (s, 2H). Anal. Calcd for **1**·DMF·3.5H₂O (C₇₃H₆₀O₈.₅Zn): C, 76.07; H, 5.25; N, 1.22. Found: C, 75.91; H, 4.45; N, 1.40. MALDI⁺-MS (CHCl₃/MeCN): m/z 1037 [M + Na]⁺.

Physical Measurements. C, H, and N analyses were performed with a Perkin-Elmer 2400 series II analyzer. Electrospray-ionization mass spectra (ESI⁺-MS) of **1** were recorded in DMF/MeOH in a Finnigan MAT 8200 spectrometer. In addition, the mass spectrum of **1** was recorded in CHCl₃/MeCN using matrix-assisted laser desorption ionization with a time-of-flight (MALDI-TOF) mass spectrometer (4800 *Plus* MALDI TOF/TOF (ABSciex -2010)). Infrared spectra (4000−400 cm^{-1}) were recorded from KBr pellets on a Bruker IFS-125 FT-IR spectrophotometer. The ^{1}H NMR spectrum was recorded at room temperature with a Mercury 400 spectrometer. Cyclic voltammograms were recorded with an EG&G potentiostat/ galvanostat in CH₂Cl₂. Cyclic voltammograms (CV) and differential pulse voltammograms (DPV) were performed on 9Accm and

complexes **1** and **2** in distilled CH₂Cl₂ using 0.1 M (NBuⁿ₄)PF₆ as supporting electrolyte and a scan rate of 100 mV/s. The analyte concentrations were 0.5 mM for 9Accm and **1** and 0.25 mM for **2**. The Fc/Fc⁺ couple was used as an internal reference. Fluorescence emission spectra were carried out on Horiba-Jobin-Yvon SPEX Nanolog-TM and Cary Eclipse spectrofluorimeters. Confocal studies were performed using a Lecia TCS_SPE: objective ×60. AFM images were captured in tapping mode using a Multimode AFM attached to a Nanoscope IV electronics (Digital Instruments, Santa Barbara, CA). Single-beam silicon oxide AFM probes were used (T300R-W series, VistaProbes, Phoenix, AZ) with a nominal spring constant of 40 nN/ nm. In order to preserve the structure of the sample, the free amplitude of the AFM probe was kept to a minimum and images were acquired at the maximum amplitude set point. The scan rate was set to 0.7 Hz, and the resolution was 512 × 512 pixels.

X-ray Structure Analysis. Data for compound **1** were collected on a small yellow block on a Bruker Kappa-Mach3/APEXII-CCD diffractometer equipped with a Mo-target rotating anode setup and an Incoatec-Helios-Mirror monochromator. Final cell constants were obtained from a least-squares fit of several thousand strong reflections. The structure was readily solved with the Patterson method and subsequent difference Fourier techniques. Refinement on F^2 was performed with the SHELXTL suite.[12] All non-hydrogen atoms were refined anisotropically. Hydrogen atoms were placed at calculated positions and isotropically refined as riding atoms.

Electron Structure Analysis. Density functional theory (DFT) calculations[13] were carried out with Gaussian 03 code[14] using the B3LYP functional[15] and 6-31G* basis set on the atoms implied in coordination (Cu, Zn, O, N) and 6-31G for C and H. Analysis was performed with the Amsterdam density functional (ADF) code[16] using triple-ζ polarized basis sets (TZP) and the Becke−Perdew functional.[17] ADF calculations were carried out to rationalize the coordination bonding and stereochemical factors. In order to keep the analysis close to the ligand-field reasons, ADF calculations were done in a restricted orbital scheme. The Gaussian calculations, used for TD-DFT (time-dependent DFT)[18] analysis of spectral patterns and photophysical mechanisms, belonged to unrestricted type. In addition, preliminary calculations were achieved with the semiempirical ZINDO/S method in the Hyperchem suite.[19]

■ RESULTS AND DISCUSSION

Synthesis and Characterization of 1. Reaction of $[Zn(O_2CMe)_2(H_2O)]$ with 2 equiv of deprotonated 9Accm in DMF provided a bright orange solution, from which a yellow solid was obtained by concentrating the solution using a rotary evaporation system. The solid was dissolved in pyridine and layered with diethyl ether; yellow crystals appeared after a few days (compound **1**). The IR spectrum shows clear evidence of Zn^{II}−9Accm coordination, revealing sharp and strong −C≡O−, −C≡C−, and C−H stretching vibration bands at 1629, 1546, and 733 cm^{-1}, in that order, characteristic of coordinated curcuminoid ligands.[20] In addition, a strong molecular ion peak with a m/z value of 1015.3 was detected by ESI⁺-MS and another of 1037.1 using MALDI-MS, indicating formation of the desired complex ([M + H⁺] and [M + Na⁺], respectively). The ^{1}H NMR spectrum (CDCl₃) of the yellow solid reveals only six signals in the aromatic region, consistent with the existence of $Zn(9Accm)_2$ species in solution possessing high symmetry, where the two 9Accm ligands are equivalent and therefore the four anthracene groups. Figure 1 depicts the spectrum as well as assignment of the peaks, and Figure S1, Supporting Information, shows the ^{1}H NMR results of free 9Accm.

In the present work, compound **1** is compared with an analogous system, $[Cu(9Accm)_2(py)]$ (**2**), to gather information on the coordination and final properties of 9Accm with metal centers. Both compounds are visually different: the Zn^{II}
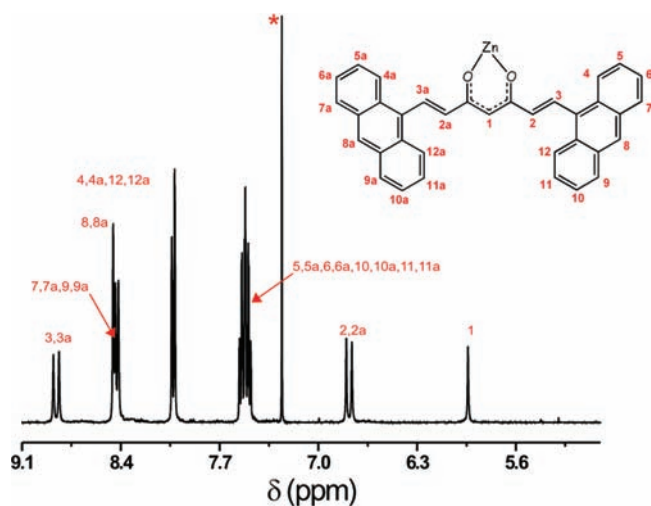
Figure 1. Aromatic region of the ^{1}H NMR of $Zn(9Accm)_2$. Asterisk (*) indicates $CDCl_3$ solvent. Numbers in red indicate protons.

powder is bright yellow, meanwhile the Cu^{II} species show an orange-brown color; such variation comes after coordination to the ligand, where free 9Accm displays a vivid red color. This ligand is a powerful dye that, once coordinated, provides colors than range between yellow and brown. On the other hand, the two coordination compounds are soluble in a variety of organic solvents but insoluble in H_2O due to the hydrophobic nature of 9Accm.

Crystal Structure [Zn(9Accm)₂(py)] (1). A labeled ORTEP representation is depicted in Figure 2. Crystallographic
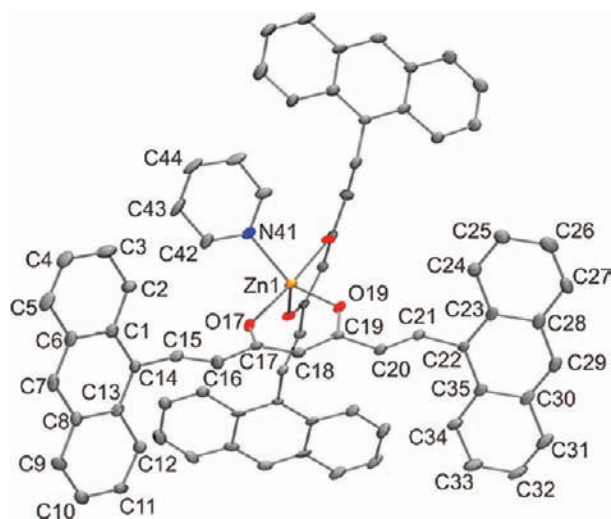
Figure 2. Coordination diagram of $[Zn(9Accm)_2(py)]$ (**1**) and atom-numbering scheme. Zinc atom is in yellow, nitrogen in blue, oxygen in red, and carbon in gray. Hydrogen atoms have been omitted for clarity.

data for compound **1** are collected in Table S1, Supporting Information.[21] The system crystallizes in the monoclinic space group C_2. Compound **1** contains a pentacoordinated Zn^{2+} ion that exhibits a distorted trigonal bipyramidal geometry, TBP ($\tau \approx 0.82$).[22] Indeed, the metal center is coordinated to four oxygen atoms from β-diketone groups of two 9Accm ligands and one nitrogen atom from a pyridine molecule occupying one of the three equatorial positions (Figures 2 and 3). The Zn–N bond length is 2.124 Å, and two types of Zn–O distances of
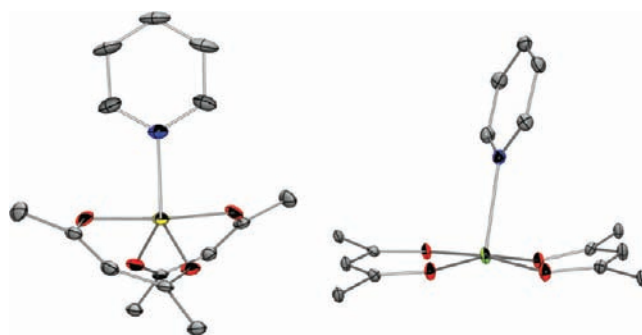
1.977 and 2.040 Å were found, similar to others in the literature (Table S2, Supporting Information).[23] The equatorial plane shows two sorts of angles, N–Zn–O of 126.05° and O–Zn–O of 107.90°, and as expected, the angle O–Zn–O formed by the oxygen atoms located in the apical positions is close to 180° (175.30°).

Related to the attached curcuminoid, both 9Accm within the molecule exhibit two main C–C distances that agree well with single (1.465–1.486 Å) and double (1.311–1.320 Å) bonds, already observed in related conjugated heptadiaryl systems.[9] In addition, the two anthracene groups in each ligand are tilted (approximately 70–73°) from the lineal conjugated skeleton opening the central part. In fact, additional anthracene groups from neighboring molecules are able to fill part of the exposed space. Regardless, no relevant interactions among clusters were found (Figure S2, Supporting Information).

Interestingly, compound **1** exhibits the same number and sort of ligands than a related Cu^{II} complex recently published by us,[9] $[Cu(9Accm)_2(py)]$ (here for comparison purposes numbered **2**). However, the coordination geometry of the Cu^{II} complex clearly differs from **1** (Figure 3); previous work has shown that complex **2** displays an ideal square pyramidal conformation (SP, τ = 0.10, Figure 3, right).[9,22] Crystallographic parameters, distances, and angles for both compounds are compared in Table S3, Supporting Information. In general, pentacoordinated Zn and Cu compounds can exhibit both geometries: SP or TBP together with intermediate arrangements.[24] Here, there is a preference for the Zn^{II} complex to display a TBP geometry instead of the SP one previously found for the Cu^{II} analog under the same recrystallization conditions (pyridine/diethyl ether). Taking into account the flexibility of the chelating ligand and the absence of strong intermolecular interactions in both compounds, the difference in stereochemistry may be guided by the electronic configuration of the metal centers, where the Jahn–Teller axis of the Cu^{II} system could play a relevant role in the structural organization, being the longest distance Cu^{II}–ligand the one related to the monodentate ligand, pyridine, appearing in the apical position.[25] In this sense, there are few mononuclear systems that, containing identical number and nature of ligands coordinated to Zn^{II} and Cu^{II} centers, display different conformation;[25] **1** and **2** are the first explored with curcuminoid ligands, giving as a result flexible metal–organic frameworks.

Also, we would like to emphasize the lack of crystallographic data for metal–curcuminoids in the literature. Certainly, complexes containing curcumin or curcuminoids have been

Figure 3. ORTEP representation of the central core of complex **1**, $[Zn(9Accm)_2(py)]$, on the left and **2**, $[Cu(9Accm)_2(py)]$, on the right. Zn atom in yellow, Cu in light green, oxygen in red, nitrogen in blue, and carbon in gray.

Table 1. Electronic Absorption and Emission Data of Compounds 9Accm, 1, and 2 in CH_2Cl_2 (10^{-5} M)

compound	absorption spectra (CH_2Cl_2) λ_{max}, nm (10^{-3} ε M^{-1} cm^{-1})	emission spectra (CH_2Cl_2) λ_{max} (nm)/λ_{exc} = 443 nm	emission spectra (solid) λ_{max} (nm)/λ_{exc} = 425 nm
9Accm	256 (127.7), 341 (8.9), 363 (8.2), 383 (7.8), 433 (9.2)	575	663
1	255 (290.3), 347sh (22.0), 365 (23.6), 384 (22.8), 441 (29.9)	580	562
2	254 (286.6), 347sh (16.1), 365sh (20.2), 386sh (23.8), 443 (43.5)	572	646
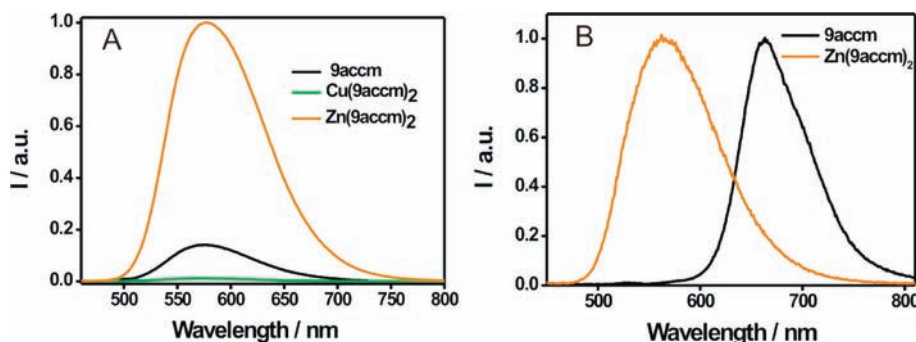
Figure 4. (A) Normalized emission spectra of 9Accm (black), complex **1** (orange), and **2** (green) in CH_2Cl_2 (10^{-5} M). (B) Normalized emission spectra in the solid state of 9Accm (black) and complex **1** (orange).

studied and published during the last decades, several of those by Krishnankutty et al.[20a,26] and Zhou et al.[20b] with a large portion on characterization and biological properties of such compounds. However, only one Ru[III][27] and two recent Cu[II] compounds[9] (the latest by our group) have been characterized crystallographically. Here, we present the first crystal structure of a Zn−curcuminoid, providing insight on the structural properties of this family of ligands. In addition, DFT calculations on complexes **1** and **2** have been performed to further analyze data exposed above.

Comparative Analyses Among 9Accm and Complexes 1 and 2. *UV−Vis Studies.* The electronic absorption spectra of 9Accm and the two metal compounds were recorded in 1×10^{-5} M dichloromethane solutions, and the results are summarized in Table 1 and Figure S3, Supporting Information. All of them present a similar pattern: two bands at ca. 250 and ca. 435 nm, typical of the curcuminoid ligands, together with the well-resolved vibrational bands of the anthracene ligands in the range 340−385 nm. Although the band at ∼250 nm has been designated as a $\pi \rightarrow \pi^*$ transition,[26c,d] the assignment of the origin of the low-energy band is not so clear. Initially, the band was attributed to the $n \rightarrow \pi^*$ electronic transition for curcumin and curcuminoids,[26c,d] although additional studies have indicated a $\pi \rightarrow \pi^*$ nature.[28] As a result, in some work it has been considered a combination of both $n \rightarrow \pi^*$ and $\pi \rightarrow \pi^*$ transitions, with the dipole-forbidden $n \rightarrow \pi^*$ absorption band buried under the strong $\pi \rightarrow \pi^*$ transition.[29] In the present work, the computational analyses with TD-DFT/B3LYP and semiempirical ZINDO/S are in agreement with a $\pi \rightarrow \pi^*$ assignment for the lowest energy transition (explanation below and in the Supporting Information).[19] Comparing the absorbance spectra of the free ligand and compounds **1** (Zn[II]) and **2** (Cu[II]) it is clear that metal binding is accompanied in both complexes by a slight red shift (∼10 nm) of the band at 433 nm (Table 1). Moreover, a change of color was observed depending on the solvents used, and at present solvatochromic experiments are being performed with all samples.

Electrochemical Studies. The results of the electrochemical experiments for 9Accm and **1** are depicted in Figure S4, Supporting Information, and in Figures S5 and S6,

Supporting Information, for **2**. All three species exhibited the same general behavior: irreversible oxidations between 1.00 and 1.85 V (approx.) and irreversible reductions between 0 and −2.30 V (data vs Fc/Fc[+]). A first approach to the understanding of the results derives from direct comparison of the voltammogram of 9Accm with the two compounds, **1** and **2**, respectively. It appears that the electrochemical features in both compounds are controlled by the nature of 9Accm, which appears unable of stabilizing when electrons are added or removed. Even though the electrochemical behavior of both compounds **1** and **2** are similar, further oxidation processes seem to appear for the Cu[II] species at high potentials (Figures S5 and S6, Supporting Information). Increasing the scan rate from 100 to 1000 mV/s leads to the observation of two quasi-reversible reduction processes for compound **1** at −1.46 and −1.59 V vs Fc/Fc[+] (Figures S4, inset, and S7, Supporting Information). In this respect, no changes were observed for compound **2**, although reduction from Cu[II] to Cu[I] are possible in other systems. Overall, these two analogous systems display similar electrochemical behavior.

Luminescence Studies. Emission spectra were recorded in CH_2Cl_2 upon excitation at 385 and 443 nm, showing broad bands around 575 nm (Figure 4A and Table 1). No emission is observed when the samples are excited at ∼250 nm. Excitation spectra collected at the maxima reproduce absorption spectra in the range 240−565 nm (see Figures S8−S10, Supporting Information), pointing out that the observed emission is originated by the 9Accm ligand (in all cases). The small Stokes shifts are indicative of a singlet parentage for these transitions. Interestingly, a slight blue shift is observed for the copper derivative (**2**), while a similar small shift is observed to the red for compound **1**. The Cu[II] system presents a marked quenching of the fluorescence emission of 9Accm (green band, Figure 4A) due to the d[9] electronic configuration of this paramagnetic metal cation (CHEQ effect). On the contrary, complex **1** displays an enhancement of the fluorescence (CHEF effect), typical of complexation with this metal atom.[24]

This effect is also noticed in the solid state where a bright yellow light is observed for **1** using a UV−vis lamp and exciting at 365 nm. In the same conditions, 9Accm depicts a bright red

color and no emission is detected for **2** (Figure 5). Solid emissions of 9Accm, **1**, and **2** are shown in Table 1, where all
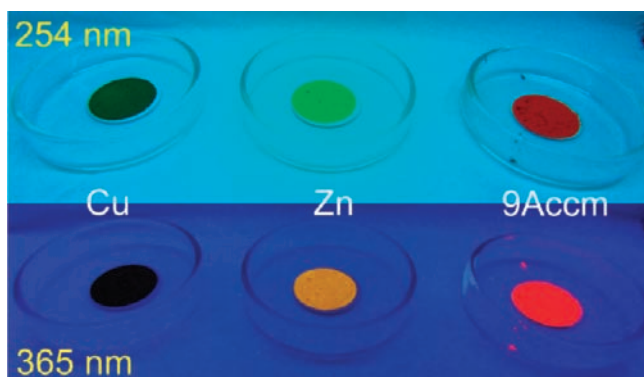
Figure 5. Solid fluorescence of 9Accm and complexes **1** (Zn) and **2** (Cu) at 254 and 365 nm, respectively.

three follow interesting trends: 9Accm depicts a strong emission peak at 663 nm, ca. 100 nm shifted to the red compared with the results in solution (Figure 4B). This could be attributed to the $\pi-\pi$ stacking effects among the molecules in the solid state. This effect is also observed in **2**, although now the emission of the copper complex is only residual (not shown). On the other hand, **1** presents a pattern that may directly correlate with its structure: the Zn derivative is strongly luminescent in the solid state; its emission maximum is 100 nm blue shifted with respect to the free ligand (solid state) and in the same range than all compounds in solution (Figure 4A). In this sense, the position of this emission band could be related to its TBP geometry that makes difficult $\pi-\pi$ stacking interactions in comparison with that observed for 9Accm and, consequently, the latest (9Accm) shifts to the red.

Nanostructuration: AFM and Confocal Studies. Due to the potential applications of the Zn^{II} compounds as fluorescent molecular devices, AFM and confocal spectroscopic experiments were performed by deposition of **1** on graphite surfaces.[4,5,8] In principle, the irreversible electrochemical nature of **1** (Figure S4, Supporting Information) may allow the study of these species in different substrates without further oxidations or reductions; however, due to the structure of the ligand, the graphite surface was chosen as an initial attempt. Certainly, the anthracene groups of the ligand provide not only fluorescent and electronic properties but also intermolecular interactions with the substrate ($\pi-\pi$ stacking) that facilitate deposition.

AFM experiments were performed with a Multimode force microscope. To optimize the sensitivity, measurements were done in noncontact phase detection mode. Deposition of **1** on the graphite surface was performed by dip coating, where the graphite substrates were immerged in solutions of **1** (1.35 × 10^{-4} and 1.35 × 10^{-5} M in CH$_2$Cl$_2$, respectively) at different periods of time (see Figures 6, 7A, and 7B). Afterward, the samples were left to dry and then measured.

Molecules of **1** seem to favor aggregates (yellow color). The bigger accumulation of those were found at the highest concentration and dipping times. On the contrary, decreasing the two parameters allowed the observation of larger extensions of uncovered graphite surface (red color, Figures 6D and 7A). AFM images of Figures 7A, 7B, and S11, Supporting Information (lowest concentration and dipping time) shows
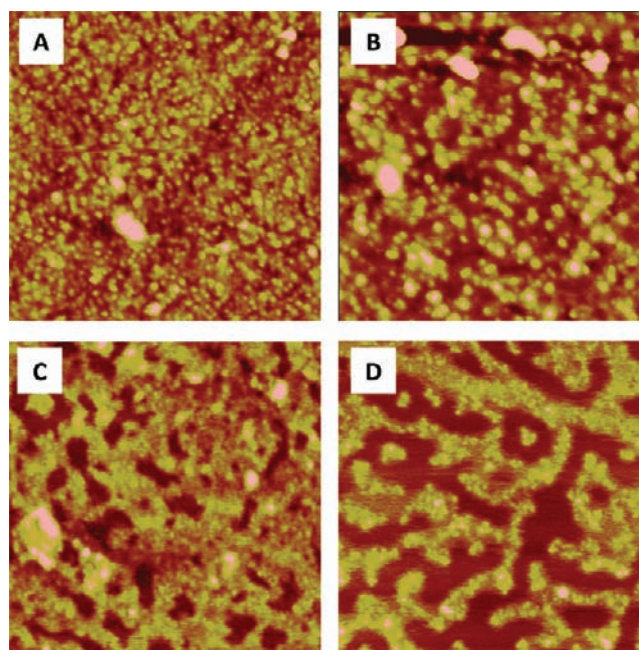
Figure 6. AFM images of molecules of **1** on a graphite surface by dip coating: (A) (500 × 500 nm) surface immersed for 2 min in a solution of **1** in CH$_2$Cl$_2$ (1.35 × 10^{-4} M), (B) (500 × 500 nm) surface immersed for 30 min solution of **1** in CH$_2$Cl$_2$ (1.35 × 10^{-4} M), (C) (500 × 500 nm) surface immersed for a few seconds in a solution of **1** in CH$_2$Cl$_2$ (1.35 × 10^{-4} M), (d) (1 × 1 μm) surface immersed for a few seconds in a diluted solution of **1** in CH$_2$Cl$_2$ (1.35 × 10^{-5} M).

accumulation of small particles but similar height, which values in most cases are between 0.8 and 3.0 nm (Figure S11, Supporting Information) correlated to just 1 or 2 pilled molecules (by strictly comparison with the molecular structure of **1**, Figure S12, Supporting Information). Molecular disposition on the substrate may be related to (i) intermolecular interactions between molecules of **1** with graphite, (ii) supramolecular interactions among themselves, and (iii) solvent evaporation processes (Figure 6). Substitution of the pyridine molecule in the axial position of **1** opens the possibility of coordination and therefore molecular recognition (e.g., functionalized surfaces).

On the other hand, fluorescence on graphite surfaces by means of confocal spectroscopy was performed using a similar sample of **1** (10^{-5} M in CH$_2$Cl$_2$, Figure 7C). In the experiment, complex **1** was added on the substrate using a drying drop approach and afterward was protected with a coverslip. Figure 7C shows the image obtained after irradiating the substrate with a light in the blue range (approximately 350 nm). In a higher scale than before (micrometers) it is possible to observe the fluorescence produced by aggregates placed on the surface. Now, molecules of **1** group together; due to the evaporation of the solvent (and therefore deposition of the molecules), microrings were formed on the graphite.

Intermolecular interactions between complex **1** and the surface are unambiguous using both AFM and confocal microscopy. At the same time, additional factors such as the solvent, concentration of the sample, and method of deposition determine the formation and size of supramolecular structures on the graphite support. Subsequent studies using STM and STM-induced electroluminescence are crucial as the next approach to further analyze the deposition of single molecules of **1** on the surface as well as their fluorescence properties as
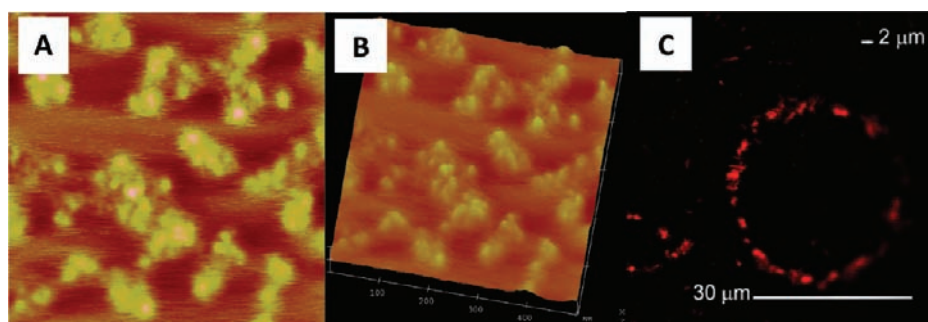
Figure 7. (A and B) AFM images of molecules of **1** on a graphite surface by dip coating (500 × 500 nm). The graphite surface was immersed for a few seconds in a solution of **1** in CH_2Cl_2 (1.35×10^{-5} M). (B) 3D representation of A. (C) Confocal microscopy image of a microdrop of complex **1** (similar images, bigger size in Figure S13, Supporting Information).

individual systems. In this sense, it is well known that $\pi-\pi$ stacking, hydrogen bonding, and immobilization on solid supports can induce quenching on the fluorescence in most conjugated organic molecules.[30] However, complex **1** could be an interesting case to analyze as a potential fluorescent device[7a,11a] on graphite or additional functionalized surfaces (covalent attachment with the substrate) due to the number of chromophores it contains (four per molecule) and the enhancement of the final fluorescence due to the Zn center.

Density Functional Theory Analysis of Structure and Bonding. With the aim of rationalizing the preference of complexes **1** (Zn^{II}) for trigonal bipyramid (TBP) and **2** (Cu^{II}) for square pyramid (SP) geometries we performed DFT calculations using specific analyses implemented in the ADF code.[31,32] Structures were optimized with symmetry idealization: C_2 for $[Zn(9Accm)_2(py)]$ and C_{2v} for the $[Cu(9Accm)_2(py)]$, with the setting mentioned in the technical section. The total bonding energy (i.e., the association energy with respect to the metal ion and ligand fragments) was divided, as a specific feature of the ADF output,[32] in several components: Pauli repulsion, electrostatic interaction, and the orbital part. The Pauli repulsion is a term of quantum nonbonding nature, resulting from the closed-shell subsystems of the fragments.[33] The electrostatic part corresponds to the classical terms from charge distribution, while orbital interactions are including elements related to quantum bonding effects. In our case, it can be used considering that it incorporates the ligand-field stabilization energy (LFSE).[34] The results are outlined in Table 2, and molecular orbital diagrams are depicted in Figures S14 and S15, Supporting Information.

The comparative analysis of data in Table 2 agrees well with ligand-field reasons: the SP structure of **2** is determined by LFSE factors, while the TBP structure of **1** is driven by minimization of interligand repulsion, missing LFSE contributions from the d^{10} metal center.[34] In terms of sterical hindrance, the TBP is the most relaxed structure, having small Pauli repulsions for both the Cu^{II} and the Zn^{II} systems. On the other hand, the orbital interaction is the driving factor of the stereochemical difference: **2** firmly favors SP geometry, prevailing over opposed trends as Pauli repulsions and electrostatic terms. The orbital interaction is slightly favorable to SP in the case of **1** too, but its relative magnitude does not encompass the other terms that strengthen TBP geometry. The orbital term leads the structural differences where the d^9 ion benefits from LFSE effects, while the d^{10} ions do not possess

Table 2. Energy Decomposition Analysis of Bonding Effects in $[M^{II}(9Accm)_2(py)]$ (M^{II} = Zn, Cu) Complexes with Trigonal Bipyramid (TBP) and Square Pyramid (SP) Complexes[a]

stereochemistry	SP	TBP	SP	TBP
symmetry	C_{2v}	C_2	C_{2v}	C_2
M^{II}	Cu^{II}	Zn^{II}	Zn^{II}	Cu^{II}
Pauli repulsion	7.339	6.522	6.721	7.114
electrostatic interactions	−24.534	−24.792	−24.597	−24.741
orbital interactions	−15.341	−12.305	−12.608	−14.569
total bonding energy	−32.536	−30.574	−30.483	−32.196

[a]The first two data columns correspond to realistic systems (Zn^{II} complex as TBP optimized with C_2 symmetry and Cu^{II} complex as SP with C_{2v} symmetry). The last two columns correspond to hypothetical reversed structures: Zn^{II} system taken at former SP structure of Cu^{II} system and vice versa. All quantities are in eV.

this contribution (Figure S16 and related notes in the Supporting Information).

Correlations with the Photophysical Properties. On this matter, we set computational experiments to explore the mechanism of luminescence in complexes **1** and **2**. The TD-DFT-computed excited states match well the experimental bands and intensities. Thus, for **1** there are four relatively intense bands at 441.0, 439.4, 379.3, and 378.4 nm. In similar conditions compound **2** shows bands at 461.2, 441.5, 377.7, and 372.7 nm. The position of the excited levels is comparable in both systems and close to the experimental bands (ca. 385 and 440 nm). Here, it should be emphasized that our goal was to compare these outcomes with the experimental results to realize qualitative aspects of the mechanism considering idealized symmetries but without aiming for quantitative evaluations. DFT optimization in these series of calculations was performed with the B3LYP functional in an unrestricted orbital setting. In order to discriminate the role of the metal ion from the effects of stereochemistry we considered the Zn^{II} and Cu^{II} complexes having the same C_{2v} idealized geometry (optimized for Cu^{II} case). As a result, it was observed that the two systems were highly similar in the position of the active transition, a fact that suggests the common nature of the excitation (due to the ligand itself, Figures S14 and S15, Supporting Information).[35]

A possible mechanism of spin-driven fluorescence quenching is illustrated in Figure 8, which compares the singlet and triplet TD-DFT states of **1** (with idealized C_{2v} symmetry) with the excited doublet states of the **2**. In the case of **1**, each singlet state has a triplet companion with identical symmetry and
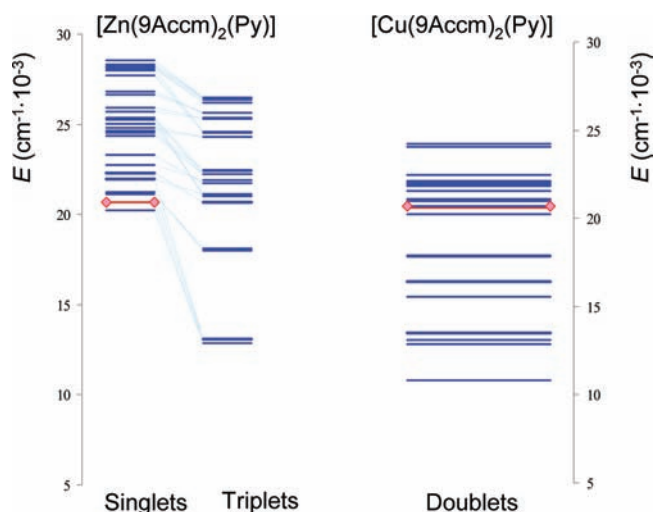
Figure 8. TD-DFT levels computed for the C_{2v} idealized complex **1** (singlet states on the left panel, triplet states on the middle panel) in comparison with **2** having the same geometry. The transition with maximal intensity is marked in both complexes by the red line and diamond symbols.

similar composition in the coefficients of orbital promotion (occupied to virtual) components. These singlet−triplet couples differ by the spin flip but determine the same charge transfer effects. Figure 8 shows that the triplet states are always sensibly lower in energy. For **1** the singlet state with the highest intensity is second in the singlet series, being marked by diamond symbols and red line (Figure 8, left side). The intense transition in **2** is indicated in the same way (right side). It happens approximately at the same energy but has several other low-lying levels below. Four of these lower TD-DFT levels are identified as d−d ligand-field-type processes (see Figures S17 and S18 and related tables in the Supporting Information). The rest of the lower states are originating from antiparallel coupling of spins from triplet states located on the ligand moieties and the unpaired electron on the Cu^{II} center. Thus, the Cu^{II} ion mediates the configuration interaction channels between singlet and triplet states located on the ligand frame that were spin forbidden in the Zn^{II} compound (**1**). After the coupling with the paramagnetic ion, both singlet and triplet series on the ligand generate levels with the same doublet spin multiplicity. The interaction with lower levels offers multiple routes for nonradiative relaxation of the excited states involved in the luminescence. In turn, **1** does not possess such lower states (or a spin-coupled mechanism to remove the singlet−triplet forbiddances) and therefore favors the luminescence by the absence of other relaxation mechanisms. The existence of spin-polarized states (originating from a triplet located on ligands

$\lambda = 441$ nm, $f = 0.24$

$\lambda = 379.3$ nm, $f = 0.22$

$\lambda = 483.2$ nm, $f = 1.07$

$\lambda = 394.7$ nm $f = 0.26$
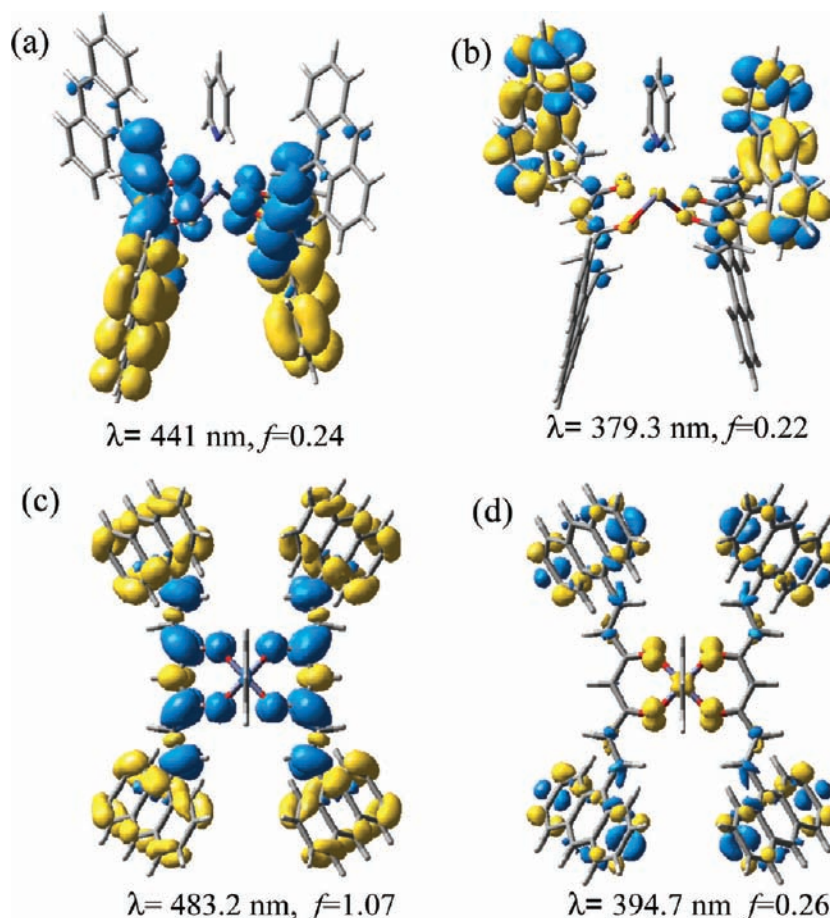
Figure 9. Density difference map for selected TD-DFT states of **1**: (a and b) most intense transitions computed at experimental geometry (TBP); (c and d) corresponding transitions in the idealized C_{2v} structure (SP). Representations correspond to the total density of the excited state minus the density at the ground state. The blue surfaces are the zones where the density moves during the transition; the yellow ones correspond to density depletion. Wavelength (λ) and relative intensity (f) of the transition are marked near each inset.

and a β spin density on metal ion) is illustrated in the Supporting Information (Figure S19).

Density difference maps between the total density at the excited state and the ground state are powerful tools for characterization of TD-DFT transitions. The contours of the excited vs ground state density difference show the displacement of electrons in parts of the molecule after a given excitation. Figure 9 depicts selected states of complex **1** (Figure 9a and 9b) and **1** in the idealized C_{2v} symmetry (Figure 9c and 9d). The lowest transition corresponds to displacement of density from the anthracene groups toward the coordination frame (C=O bonds) and the C=C double bonds that link the two anthracene groups to the β-diketone moiety. The higher transition is a reverted process, from the oxygen atoms of the β-diketone groups toward the anthracene units, combined with orbital rearrangements in the peripheral groups. Qualitatively, the charge displacements are the same in both real and idealized systems. The latest shows equal contributions (C_{2v} system), while the former (lower symmetry) displays one anthracene group per ligand predominantly involved. These patterns confirm the initially assumed $\pi \rightarrow \pi$ nature of the relevant optical absorptions. Besides, a comparison of the idealized C_{2v} complex **1** with the isostructural compound **2** showed similarities on the transitions, confirming that the important transitions are due to the ligand itself, with rather indirect implication of the metal ion (Figures S20−S22 and explanation in the Supporting Information).

■ CONCLUDING REMARKS

Following previous work with ligand 9Accm (anthracene-based curcuminoid), a new complex containing the curcuminoid system attached to a Zn^{II} center is now presented. Once more, it the capacity of 9Accm for coordination purposes as well as its contribution in the inherent treats of the final compound has been proved. Here, we synthesized mononuclear species where zinc binds two 9Accm ligands and one molecule of pyridine, [Zn(9Accm)$_2$(py)] (**1**). The crystal structure of **1** is the first describing Zn−curcuminoid species in the literature. Interestingly, this complex displays a quasi-ideal bipyramidal trigonal arrangement unlike a preceding similar copper compound, [Cu(9Accm)$_2$(py)] (**2**), which shows a square pyramidal environment. The conformational differences among them have been discussed in terms of Jahn−Teller effects in the Cu^{II} centers, and theoretical studies have been performed to confirm their geometries. We would like to emphasize that there is a growing amount of literature and patents which deal with the possible applications of these complexes in bioinorganic areas. However, this work aims to show the potential use of these compounds as components of molecular devices as well. Toward this goal, further experiments have been performed with the following outcomes: (i) electrochemical studies of 9Accm, **1**, and **2** in CH_2Cl_2 have shown that their electronic behavior depends on the ligand displaying all three irreversible oxidations and reductions; only complex **1** shows semireversible reduction waves at high scan rates; (ii) fluorescence assays in the same solvent indicate that **1** exhibits a chelation enhancement of fluorescence (CHEF) and **2** a chelation enhancement of quenching (CHEQ) with respect to the fluorescence response of the free ligand, showing that 9Accm has a high-sensitivity response upon coordination; (iii) fluorescence in the solid indicates that supramolecular interactions may explain the strong shift toward the red area of the spectrum for 9Accm, meanwhile **1** presents an emission

comparable to the solution experiments; (iv) deposition of complex **1** by deep coating (CH_2Cl_2) on graphite shows on average small assemblies of molecules among them and distribution all over the surface mainly due to supramolecular interactions ($\pi-\pi$ stacking) and (v) on the same support but in a higher scale, confocal microscopy has shown fluorescent emission and similar arrangements for the molecules.

Electron structure calculations and idealized computation experiments were used to understand the different features described in the Experimental Section. Energy decomposition analysis offered a clear rationalization for the stereochemical preferences of the compared systems, **1** and **2**. The square pyramidal pattern is stabilized by ligand-field factors of the d^9 configuration of the Cu^{II} ion, whereas the trigonal bipyramidal structure is determined by minimization of interligand repulsion.

A series of TD-DFT calculations on idealized systems offered a suitable explanation for the different photochemical behavior of **1** and **2** compounds and proposed mechanisms for their photophysical properties. The luminescence of the Zn^{II} system is favored by the fact that the involved states are among the first excited levels of the spectrum. In turn, placed at comparable energy to those of the Zn^{II} analogue, the active levels of the Cu^{II} complex are not the first ones. The manifold of states with lower energy determines enhanced configuration interaction coupling and multiple channels of nonradiative decay. The low-lying states are of ligand-field type and of spin-polarized nature. In particular, the spin-polarized levels resulted from antiparallel coupling of a triplet state located on the ligands, and the β electron on the highest d-type MO are regarded as the factors to remove the spin-forbidden relaxation. Detailed analysis together with the use of density difference maps (excited state vs ground state) identified the nature of the significant transitions involved in absorption and emission processes. The charge displacements occur from anthracene groups toward the diketonate and olefinic moieties of the ligand. This conclusion appears in both idealized systems and experimental structures. With all the above results we demonstrated that the approach of designing small molecules able to assemble features from the attached ligands, and metals can lead to novel luminescent materials providing, in some cases, dramatic changes on their optical properties.

■ ASSOCIATED CONTENT

ⓢ Supporting Information

Crystallographic details of compounds **1** and **2**, crystallographic packing diagram of compound **1** and general intramolecular distances, UV−vis spectra of 9Accm, **1**, and **2** in CH_2Cl_2; isodensity representation of the orbitals of 9Accm; cyclic voltrammograms of compounds **1** and **2**; normalized excitation spectra of 9Accm, **1**, and **2**; solid fluorescence pictures; additional AFM and confocal images of **1**; details on DFT and TD-DFT calculations and further relevant discussion related with the modeling. This material is available free of charge via the Internet at http://pubs.acs.org. Crystallographic data files (cif format) for compound **1** have been deposited at the Cambridge Crystallographic Data Centre and allocated the deposition number CCDC 832819. This material is available free of charge via the Internet at http://www.ccdc.cam.ac.uk/data_request/cif.

AUTHOR INFORMATION

Corresponding Author
*E-mail: nuria.aliaga@icrea.cat.

REFERENCES

(1) (a) Li, S.-S.; Northrop, B. H.; Yuan, Q.-H.; Wan, L.-J.; Stang, P. J. *Acc. Chem Rev.* **2008**, *42*, 249. (b) Canary, J. W.; Mortezaei, S.; Liang, J. *Coord. Chem. Rev.* **2010**, *254*, 2249. (c) Wagenknecht, P. S.; Ford, P. C. *Coord. Chem. Rev.* **2011**, *255*, 591. (d) Geddes, C. D.; Lakowicz, J. R. *Topics in Fluorescence Spectroscopy*; Springer: New York, 2005; Vol. 9.

(2) (a) Zhang, G.; Yang, G.; Wang, S.; Chen, Q.; Ma, J. S. *Chem.—Eur. J.* **2007**, *13*, 3630. (b) Shekhah, O.; Liu, J.; Fischer, R. A.; Wöll, Ch. *Chem. Soc. Rev.* **2011**, *40*, 1081. (c) Noy, A. *Adv. Mater.* **2011**, *23*, 807.

(3) (a) Hu, J.; Lin, R.; Yip, J. H. K.; Wong, K.-Y.; Ma, D.-L.; Vittal, J. J. *Organometallics* **2007**, *26*, 6533. (b) Sun, J.; Zhang, B.; Katz, H. E. *Adv. Funct. Mater.* **2011**, *21*, 29. (c) Ma, S. Q.; Sun, D. F.; Simmons, J. M.; Collier, C. D.; Yuan, D. Q.; Zhou, H. C. *J. Am. Chem. Soc.* **2008**, *130*, 1012.

(4) (a) Malliaras, G.; Friend, R. *Phys. Today* **2005**, *58* (5), 53. (b) Kwon, J.; Kim, M. K.; Hong, H.-P.; Lee, W.; Noh, S.; Lee, C.; Lee, S.; Hong, J.-I. *Org. Electron* **2010**, *11*, 1288. (c) Marrocchi, A.; Silvestri, F.; Seri, M.; Facchetti, A.; Taticchi, A.; Marks, T. J. *Chem. Commun.* **2009**, 1380.

(5) (a) Cano, M.; Rodríguez, L.; Lima, J. C.; Pina, F.; Dalla Cort, A.; Pasquini, C.; Schiaffino, L. *Inorg. Chem.* **2009**, *48*, 6229−6235. (b) Pedras, B.; Oliveira, E.; Santos, H.; Rodríguez, L.; Crehuet, R.; Avilés, T.; Capelo, J. L.; Lodeiro, C. *Inorg. Chim. Acta* **2009**, *362*, 2627−2635. (c) Rodríguez, L.; Lima, J. C.; Parola, A. J.; Pina, F.; Meitz, R.; Aucejo, R.; García-España, E.; Llinares, J. M.; Soriano, C.; Alarcón, J. *Inorg. Chem.* **2008**, *47*, 6173−6183. (d) Rodríguez, L.; Lodeiro, C.; Lima, J. C.; Crehuet, R. *Inorg. Chem.* **2008**, 4952−4962. (e) Palacios, M. A.; Wang, Z.; Montes, V. A.; Zyryanov, G. V.; Anzenbacher, P. J. *J. Am. Chem. Soc.* **2008**, *130*, 10307.

(6) (a) Cockrell, G. M.; Zhang, G.; VanDerveer, D. G.; Thummel, R. P.; Hancock, R. D. *J. Am. Chem. Soc.* **2008**, *130*, 1420. (b) Hilderbrand, S. A.; Lim, M. H.; Lippard, S. J. *Top. Fluoresc. Spectrosc.* **2005**, *9*, 163. (c) Purrello, R.; gurrieri, S.; Lauceri, R. *Coord. Chem. Rev.* **1999**, *190−192*, 683.

(7) (a) Alves, S.; Pina, F.; Albelda, M. T.; García-España, E.; Soriano, C.; Luis, S. V. *Eur. J. Inorg. Chem.* **2001**, 405. (b) Mameli, M.; Aragoni, M. C.; Arca, M.; Caltagirone, C.; Demartin, F.; Farruggia, G.; De Filippo, G.; Devillanova, F. A.; Garau, A.; Isaia, F.; Lippolis, V.; Murgia, S.; Prodi, L.; Pintus, A.; Zaccheroni, N. *Chem.—Eur. J.* **2010**, *16*, 919. (c) Qiu, Y.; Wang, K.; Liu, Y.; Deng, H.; Sun, F.; Cai, Y. *Inorg. Chim. Acta* **2007**, *360*, 1819.

(8) (a) Huang, C.-Y.; Su, Y. O. *Dalton Trans.* **2010**, *39*, 8306. (b) Gao, L.; Wang, Y.; Wang, J.; Huang, L.; Shi, L.; Fan, X.; Zou, Z.; Yu, T.; Zhu, M.; Li, Z. *Inorg. Chem.* **2006**, *45*, 6844. (c) Ojida, A.; Takashima, I.; Kohira, T.; Nonaka, H.; Hamchi, I. *J. Am. Chem. Soc.* **2008**, *130*, 12095. (d) Drewry, J. A.; Gunning, P. T. *Coord. Chem. Rev.* **2011**, 459.

(9) Aliaga-Alcalde, N.; Marqués-Gallego, P.; Kraaijkamp, M.; Herranz-Lancho, C.; den Dulk, H.; Görner, H.; Roubeau, O.; Teat, S. J.; Weyhermüller, T.; Reedijk, J. *Inorg. Chem.* **2010**, *49*, 9655.

(10) DOI: 10.1021/nl202065x http://pubs.acs.org/doi/abs/10.1021/nl202065x.

(11) (a) Kim, S.-H.; Gwon, S.-Y.; Burkinshaw, S. M.; Son, Y.-A. *Spectrochim. Acta, Part A* **2010**, *76*, 384. (b) Bronson, R. T.; Michaelis, D. J.; Lamb, R. D.; Husseini, G. A.; Farnsworth, P. B.; Linford, M. R.; Izatt, R. M.; Bradshaw, J. S.; Savage, P. B. *Org. Lett.* **2005**, *7*, 1105.

(12) Sheldrick, G. M. *Acta Crystallogr., Sect. A* **2008**, *64*, 112.

(13) Koch, W.; Holthausen, M. C. *A Chemist's Guide to Density Functional Theory*; Wiley-VCH GmbH: Weinheim, 2001.

(14) Frisch, M. J.; Trucks, G. W.; Schlegel, H. B.; Scuseria, G. E.; Robb, M. A.; Cheeseman, J. R.; Montgomery, J. J. A.; Vreven, T.; Kudin, K. N.; Burant, J. C.; Millam, J. M.; Iyengar, S. S.; Tomasi, J.; Barone, V.; Mennucci, B.; Cossi, M.; Scalmani, G.; Rega, N.; Petersson, G. A.; Nakatsuji, H.; Hada, M.; Ehara, M.; Toyota, K.; Fukuda, R.; Hasegawa, J.; Ishida, M.; Nakajima, T.; Honda, Y.; Kitao, O.; Nakai, H.; Klene, M.; Li, X.; Knox, J. E.; Hratchian, H. P.; Cross, J. B.; Bakken, V.; Adamo, C.; Jaramillo, J.; Gomperts, R.; Stratmann, R. E.; Yazyev, O.; Austin, A. J.; Cammi, R.; Pomelli, C.; Ochterski, J. W.; Ayala, P. Y.; Morokuma, K.; Voth, G. A.; Salvador, P.; Dannenberg, J. J.; Zakrzewski, V. G.; Dapprich, S.; Daniels, A. D.; Strain, M. C.; Farkas, O.; Malick, D. K.; Rabuck, A. D.; Raghavachari, K.; Foresman, J. B.; Ortiz, J. V.; Cui, Q.; Baboul, A. G.; Clifford, S.; Cioslowski, J.; Stefanov, B. B.; Liu, G.; Liashenko, A.; Piskorz, P.; Komaromi, I.; Martin, R. L.; Fox, D. J.; Keith, T.; Al-Laham, M. A.; Peng, C. Y.; Nanayakkara, A.; Challacombe, M.; Gill, P. M. W.; Johnson, B.; Chen, W.; Wong, M. W.; Gonzalez, C.; Pople, J. A. *Gaussian 03*, Revision C.02; Gaussian, Inc.: Wallingford, CT, 2004.

(15) (a) Lee, C.; Yang, W.; Parr, R. G. *Phys. Rev. B* **1988**, *37*, 785. (b) Becke, A. D. *J. Chem. Phys.* **1993**, *98*, 5648.

(16) *ADF2010.01, SCM*; Theoretical Chemistry, Vrije Universiteit: Amsterdam, The Netherlands, http://www.scm.com

(17) (a) Becke, A. D. *Phy. Rev. A* **1988**, *38*, 3098−3100. (b) Perdew, J. P. *Phys. Rev. B* **1986**, *33*, 8822−8824. (c) Perdew, J. P. *Phys. Rev. B* **1986**, *34*, 7406.

(18) (a) Stratmann, R. E.; Scuseria, G. E.; Frisch, M. J. *J. Chem. Phys.* **1998**, *109*, 8218. (b) Bauernschmitt, R.; Ahlrichs, R. *Chem. Phys. Lett.* **1996**, *256*, 454. (c) Casida, M. E.; Jamorski, C.; Casida, K. C.; Salahub, D. R. *J. Chem. Phys.* **1998**, *108*, 4439.

(19) *HYPERCHEM*, Version 7.0; Hypercube Inv.: Gainsville, FL

(20) (a) Krishnankutty, K.; John, V. D. *Synt. React. Inorg. Met-Org. Nano-Met. Chem.* **2003**, *33*, 343. (b) Zhao, X.-Z.; Jiang, T.; Wang, L.; Yang, H.; Zhang, S.; Zhou, P. *J. Mol. Struct.* **2010**, *984*, 316.

(21) Crystallographic data and collection parameters for complex **1** summarized as follows: formula $C_{75}H_{51}NO_4Zn$; fw 1095.54; space group *C2*; *a* 23.545(16) Å; *b* 8.979(6) Å; *c* 13.021(9) Å; *α* 90.00°; *β* 91.567(15)°; *γ* 90.00°; *V* 2752(3) Å^3; *Z* 2; *T* 100(2) K; *λ*(Mo K*α*) 0.71073 Å; ρ_{calcd} 1.322 g·cm^{-3}; *μ*(Mo K*α*) 0.502 mm^{-1}; *R* 0.0638; *ωR*^{2} 0.1284.

(22) Addison, A. W.; Rao, T. N.; Reedijk, J.; Vanrijn, J.; Verschoor, G. C. *J. Chem. Soc., Dalton Trans.* **1984**, 1349.

(23) (a) Granifo, J.; Vargas, M.; Garland, M. T.; Ibáñez, A.; Gaviño, R.; Baggio, R. *Inorg. Chem. Commun.* **2008**, *11*, 1388. (b) Clegg, J. K.; Bray, D. J.; Gloe, K.; Gloe, K.; Hayter, M. J.; Jolliffe, K. A.; Lawrance, G. A.; Meehan, G. V.; McMurtrie, J. C.; Lindoy, L. F.; Wenzel, M. *Dalton Trans.* **2007**, 1719. (c) Ali, H. M.; Halim, S. N. A.; Koushik, S.; Lajis, N. Hj.; Basirun, W. J.; Ng, S. W. *Acta Crystalogr., Sect. E* **2005**, *E61*, m691. (d) Massue, J.; Bellec, N.; Chopin, S.; Levillain, E.; Toisnel, T.; Clérac, R.; Lorcy, D. *Inorg. Chem.* **2005**, *44*, 8740. (e) Anthony, S. P.; Raghavaiah, P.; Radhakrishnan, T. P. *Cryst. Growth Des.* **2003**, *3*, 631. (f) Anthony, S. P.; Radhakrishnan, T. P. *Chem. Commun.* **2001**, 931.

(24) (a) Dong, W.-K.; Sun, Y.-X.; Zhang, Y.-P.; Li, L.; He, X.-N.; Tang, X.-L. *Inorg. Chim. Acta* **2009**, *362*, 117. (b) Wu, H.; Yun, R.; Ding, J.; Yuan, J. *Synt. React. Inorg, Met.-Org. Nano-Met. Chem.* **2008**, *38*, 604. (c) Ivanov, A. V.; Kritikos, M.; Antzutkin, O. N.; Forsling, W. *Inorg. Chim. Acta* **2001**, *321*, 63. (d) Soldatov, D. V.; Enright, G. D.; Ratcliffe, C. L.; Henegouwen, A. T.; Ripmeester, J. A. *Chem. Mater.* **2001**, *13*, 4322. (e) Borardman, A.; Small, W. H.; Worrall, I. J. *Acta Cyrstallogr., Sect. C* **1983**, *39*, 1005.

(25) (a) Nicholson, G. A.; Petersen, J. L.; McCormick, B. J. *Inorg. Chem.* **1982**, *21*, 3274. (b) Schlager, O.; Wieghardt, K.; Nuber, B. *Inorg. Chem.* **1995**, *34*, 6449. (c) Yuan, H. Q.; Aoki, K.; Fujisawa, I. *Inorg. Chim. Acta* **2009**, *362*, 975. (d) Ray, N.; Hathaway, B. *J. Chem. Soc., Dalton* **1980**, 1105. (e) Ray, N. J.; Hathaway, B. J. *Acta Crystallogr.* **1978**, *B34*, 3224. (f) Lim, B. S.; Holm, R. H. *Inorg. Chem.* **1998**, *37*, 4898. (g) Makowska-Grzyska, M. M.; Szajna, E.; Shipley, C.; Arif, A. M.; Mitchell, M. H.; Halfen, J. A.; Berreau, L. M. *Inorg. Chem.* **2003**, *42*, 7472. (h) Cao, D.-K.; Xie, X.-J.; Li, Y.-Z.; Zheng, L.-M. *Dalton Trans.* **2008**, 5008. (i) Freire, E.; Vega, D. R. *Acta Crystallogr., Sect. E* **2009**, *65*, m1430. (j) Lindoy, L. F.; McMurtrie, J. C.; Schilter, D. *Acta Crystallogr., Sect. E* **2006**, *62*, m1142. (k) Anthony, S. P.; Radhakrishnan, T. P. *Chem. Commun.* **2001**, 931. (l) Lennartson, A.; Håkansson, M.; Jagner, S. *New J. Chem.* **2007**, *31*, 344. (m) Brahma, S.; Srinidhi, M.; Shivashankar, S. A.; Narasimhamurthy, T.; Rathore, R. S. *Acta Crystallogr., Sect. E* **2011**, *67*, m819.

(26) (a) John, V. D.; Krishnankutty, K. *Main Group Met. Chem.* **2010**, *33*, 157. (b) Krishnankutty, K.; John, J.; Joseph, B. *J. Ind. Chem. Soc.* **2007**, *84*, 478. (c) John, V. D.; Krishnankutty, K. *App. Organomet. Chem.* **2006**, *20* (8), 477. (d) John, V. D.; Krishnankutty, K. *Transition Met. Chem.* **2005**, *30* (2), 229. (e) Krishnankutty, K.; Venugopalan, P. *Synt. React. Inorg. Met.-Org. Chem.* **1998**, *28* (8), 1313.

(27) Kuhlwein, F.; Polborn, K.; Beck, W. *Z. Anorg. Allg. Chem.* **1997**, *623*, 1211.

(28) (a) Zsila, F.; Bikadi, Z.; Simonyi, M. *Biochem. Biophys. Res. Commun.* **2003**, *301*, 776−782. (b) Priyadarsini, K.I. *J. Photochem. Photobiol. C: Photochem. Rev.* **2009**, *10*, 81−95.

(29) Párkányi, C.; Stem-Beren, M. R.; Martínez, O. R.; Aaron, J.-J.; Bulaceanu-MacNair, M.; Arrieta, A. F. *Spectrochim. Acta, Part A* **2004**, *60*, 1805−1810.

(30) (a) Hoeben, F. J. M.; Zhang, J.; Lee, C. C.; Pouderoijen, M. J.; Wolffs, M.; Würthner, F.; Schenning, A. P. H.J.; Meijer, E. W.; De Feyter, S. *Chem.—Eur. J.* **2008**, *14*, 8579. (b) Yang, J.-S.; Swager, T. M. *J. Am. Chem. Soc.* **1998**, *120*, 11864. (c) Jenkhe, S. A.; Osaheni, J. A. *Science* **1994**, *265*, 765.

(31) (a) te Velde, G.; Bickelhaupt, F. M.; van Gisbergen, S. J. A.; Fonseca Guerra, C.; Baerends, E. J.; Snijders, J. G.; Ziegler, T. *J. Comput. Chem.* **2001**, *22*, 931−967. (b) Fonseca Guerra, C.; Snijders, J. G.; te Velde, G.; Baerends, E. J. *Theor. Chem. Acc.* **1998**, *99*, 391−403.

(32) Dykstra, C. E.; Frenking, G.; Kim, K. S.; Scuseria, G. E. *Theory and Applications of Computational Chemistry*; Elsevier B. V.: Amsterdam, 2005; p 291.

(33) Gritsenko, O. V.; Schipper, P. R. T.; Baerends, E. J. *Phys. Rev. A* **1998**, *57*, 3450.

(34) (a) Figgis, B. N.; Hitchman, M. A. *Ligand Field Theory and its Applications*; Wiley-VCH: New York, 2000. (b) Solomon, E. I.; Lever, A. B. P. *Inorganic Electronic Structure and Spectroscopy*; Wiley & Sons, New York, 1999.

(35) The lowest band carrying intensity is located at 483.7 nm in the Cu^{II} complex and has a computed intensity of about 1.2 au. In the Zn^{II} hypothetical congener there is a transition at the same position, 483.2 nm, a bit less intense (1.07 au), and a satellite at 473.5 nm with a residual intensity (0.18 au).